Cell Communication and Signaling

RESEARCH Open Access

Mesenchymal stem cell derived extracellular vesicles reverses neural aging via OSKM modulation

Chul Kim[1], Soo-Hyeon Nam[2], Jae Hyun Park[2], Chul-Woo Lim[2], Jin Young Lee[1,2], Yun-Hwa Jeong[1], Youngsook Song[2], Moonbeom Choi[2], Seungmin Lee[2], Ji Hyung Chung[2] and Jisook Moon[1,2*]

Abstract

Background Intravenously infused human placenta-derived mesenchymal stem cells enhance overall function and exhibit therapeutic potential even with minimal engraftment or tissue replacement, with substances released from human placenta-derived mesenchymal stem cells playing a significant role in these positive outcomes. Stem cell-derived extracellular vesicles transfer beneficial factors that aid recovery in various tissues through genetic regulation. However, the effects of systemically injected mesenchymal stem cells and their released derivatives on normal aging have not been reported.

Methods Aged female mice received intravenous infusions of human placenta-derived mesenchymal stem cells. Starting at 18–19 months of age, mice were given injections of either human placenta-derived mesenchymal stem cells or PBS, followed by two more injections at six-week intervals. For the in vitro study, human fetal neural progenitor cells were sourced from spontaneously aborted fetal brain tissue. Extracellular vesicles were isolated from the human placenta-derived mesenchymal stem cell culture media using the qEV original size exclusion column.

Results RNA sequencing showed human placenta-derived mesenchymal stem cells' effectiveness in modulating aging-related neural pathways, particularly by downregulating age-specific genes in the hippocampus, indicative of neural reactivation. A pivotal aspect of our study was the discovery of micro RNAs in human placenta-derived extracellular vesicles reactivating senescent cells, likely through inhibition of Toll-like receptor 4 signaling and a concomitant increase in OSKM (OCT4, SOX2, KLF4, C-MYC) transcription factors, notably SOX2. The regeneration process involves targeted miRNAs modulating Toll-like receptor 4 and messenger RNAs boosting OSKM levels.

Conclusions Our study represents a pioneering achievement in regenerative medicine, demonstrating the potential of micro RNAs in EVs to stimulate OSKM, a significant stride forward in addressing neural aging.

Keywords Human placenta-derived mesenchymal stem cell, Extracellular vesicles, Brain aging, Toll-like receptor 4, MicroRNA, OSKM factors

*Correspondence:
Jisook Moon
jmoon@cha.ac.kr
[1]RE-CODE, 43, Beolmal-ro 30beon-gil, Bundang-gu, Seongnam-si 13503, Gyeonggi- do, Republic of Korea
[2]Department of Biotechnology, College of Life Science, CHA University, 13488 Seongnam, Gyeonggi-do, Korea

Background

Aging, a primary risk factor for senility, is characterized by a progressive decline of structural integrity and physiological functions over time. Many aging-associated markers have been identified and monitored in diverse aging-related diseases, including Alzheimer's disease (AD) and Parkinson's disease (PD), to determine their pathophysiology and to develop diagnostic tools and therapeutic interventions [1, 2]. Some of these interventions, such as modulators of immune responses, dismissal of damaged and senescent cells, and infusion with young blood, have been confirmed to extend the healthy lifespan of some animals [3–5]. Recently, the feasibility of stem cell-based therapies has been tested in several degenerative diseases, such as AD, PD, and cardiac degeneration; these therapies have produced favorable outcomes even without full replacement of the damaged tissues or cells, suggesting that the factors derived from the transplanted cells are more critical to therapeutic efficacy [6–9].

Our previous research, in conjunction with other reports, indicate that intravenously infused human placenta-derived mesenchymal stem cells (hpMSCs) not only enhance overall function but also exhibit therapeutic potential, even with minimal engraftment or tissue replacement, demonstrating released substances from hpMSCs play a significant role in driving these positive outcomes [10–12]. In addition, conditioned media (CM) from stem cell cultures are able to enhance recovery of the damaged tissues and cells in animal models, implying that bioactive materials secreted from stem cells can modulate and recover the aging process and age-associated functional deficits [13]. Among the released materials, extracellular vesicles (EVs) from stem cells were reported to transfer positive factors inducing a recovery from Huntington's disease [14]. EVs are nanoscale lipid membrane-bound particles that are released from the plasma membrane of almost all types of cells. EVs contain cell-derived proteins, peptides, nucleic acids such as DNA fragments, messenger RNAs (mRNAs), and microRNAs (miRNAs), and, via exchange of their cargos, contribute to cellular communication and modulation of neighboring cells' behaviors including development, immune responses, tumorigenesis, and disease progression [15, 16]. In particular, miRNAs in stem cell-derived EVs play important roles in the recovery processes via genetic regulation in diverse tissues such as the hypothalamus [17], blood vessels [18], kidneys [19], liver [20], and myocardial tissue [21]. However, the effects of systemically injected MSCs and their released derivatives on normal aging have not been reported.

In our pursuit to understand the potential modulation of normal aging by stem cells and their secreted elements, we initiated a regimen of intravenous injections of hpMSCs into aged mice, with subsequent administrations every six weeks. Compared to their age-matched counterparts, this regimen notably improved cognitive and locomotor functions in the aged mice manifesting enhanced neuronal signaling pathways and a reduced expression of genes typically associated with aging in the hippocampus. Moreover, we found that both the direct coculture with hpMSCs and their extracellular vesicles human placenta-derived extracellular vesicle (hpEV) treatment significantly retarded the cellular senescence in human primary fetal neural progenitor cells (hfNPCs). miRNA-rich hpEVs, as revealed through comprehensive analysis and in vitro experiments, have a profound ability to mitigate senescence and protect cells. This protection is associated with dampened Toll-like receptor 4 (TLR4) signaling and a significant upregulation of OSKM pluripotent transcription factors (*OCT4*, *SOX2*, *KLF4*, and *C-MYC*). Notably, the expression of *SOX2*, a factor closely associated with neural cells, was especially increased. This regenerative mechanism is further validated by the delivery of miRNAs that target *TLR4* signaling, complemented by the incorporation of mRNAs that enhance OSKM concentrations, setting the stage for innovative anti-aging therapeutic strategies.

Materials and methods

Animals

In our aging study, 2-month-old female mice were obtained from Orient-Bio, Inc. (Seongnam-si, Korea) and aged until 18–19 months before receiving hpMSC injections. They were housed in standard conditions with a 12/12-hour light/dark cycle and had free access to food and water. All procedures were approved by the CHA University Institutional Animal Care and Use Committee (IACUC number: 150007), following standard animal care guidelines. Female mice were chosen for their calmer temperament and longer median lifespan compared to males, which suited our long-term study needs and ensured an adequate number of subjects for the experiments [22, 23].

Isolation and culture of HpMSCs

First-trimester placental tissues (6–8 weeks' gestation) were obtained from healthy donors with comparable maternal age and no known medical complications, under Institutional Review Board (IRB)–approved protocols of the Goeunbit Hospital IRB (Republic of Korea). Written informed consent was obtained from each donor prior to tissue procurement. All placentas were processed within 30 min of delivery using a standardized enzymatic digestion protocol, as described previously by Kim et al. [10].

To minimize donor-related variability and ensure batch-to-batch consistency, only three donor placentas

were selected for hpMSC isolation. Early-passage hpMSCs (passage 5–10) were used throughout the study to avoid senescence-associated heterogeneity. All cells were expanded under identical conditions in EV-depleted medium. hpMSCs were seeded at a consistent density and cultured to approximately 80–90% confluency (not fully confluent) before harvesting. Conditioned media were collected after 48 h of culture for EV isolation.

Isolation and characterization OfEVs from HpMSC culture media

hpMSCs were seeded at consistent density and cultured to 90–100% confluency in EV-depleted media. Conditioned media were collected after 48 h and subjected to sequential centrifugation and filtration. EVs were isolated using the qEV original size exclusion column (Izon Science Ltd, Burnside, Christchurch, New Zealand) with particle-free phosphate buffered saline (PBS) as the elution buffer. Fractions 7 to 10, known to be enriched in extracellular vesicles, were pooled and further purified by centrifugation at 1,000 ×g for 1 min using a 0.22 μm Ultrafree centrifugal filter (Merk Millipore, Burlington, MA, USA).

All EV isolation procedures were carried out using rigorously standardized conditions across different hpMSC batches. To validate the consistency of EV quality between donors, we performed small RNA and mRNA sequencing analyses of hpEVs derived from each donor. In accordance with the MISEV2018 guidelines and recent ISEV2023 recommendations, the term "extracellular vesicles (EVs)" is used throughout this study to avoid assumptions about vesicle biogenesis pathways. Based on their size, morphology, and protein composition, the isolated vesicles correspond to the "small EV" category (< 200 nm).

Intravenous administration of HpMSCs to aged mice and tissue collection

Aged female mice received intravenous infusions of hpMSCs (1×10^5/100 μL PBS) via the tail vein (Fig. 1A). Starting at 18–19 months of age, mice were given injections of either hpMSCs or PBS, followed by two more injections

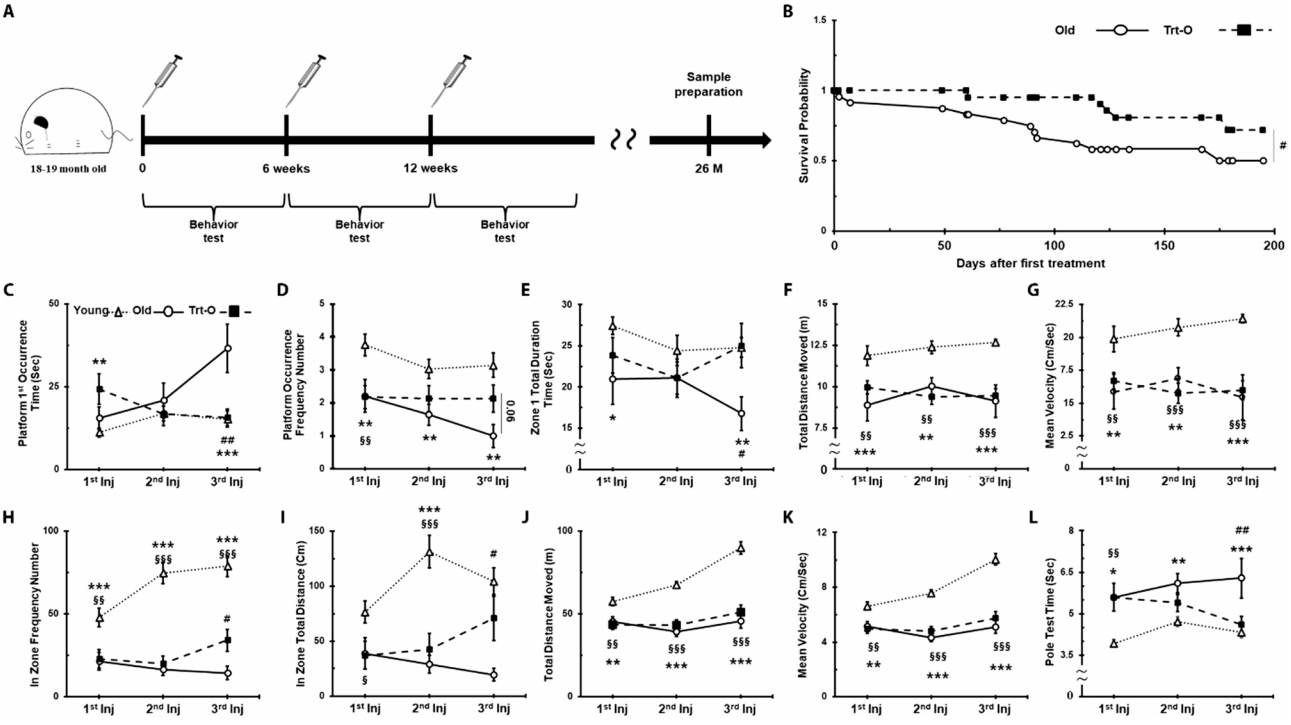

Fig. 1 Infusion of hpMSC Enhances Viability, Spatial Memory, and Cognitive Functions in Normally Aged Mice. (**A**) Schematic representation of the in vivo experiment. A total of 1×10^5/100 μl hpMSCs was intravenously injected into 18–19-month-old mice. This was followed by two more infusions every 6 weeks. Behavioral tests were performed thrice during the intervals between injections. (**B**) Multiple infusions of hpMSCs elevated the survival probability of the Treated Old mice (Trt-O) in comparison to the Old mice. (**C-G**) Multiple infusions of hpMSCs enhanced the spatial memory of Trt-O mice as seen in the MWM test: (**C**) Time of the first appearance on a test platform, (**D**) Frequency of appearances on the platform, (**E**) Duration spent in Zone 1 where the test platform was positioned, (**F**) Total distance moved, and (**G**) mean velocity were measured. (**H-K**) Locomotive and motor activity was enhanced in Trt-O mice: (**H**) Number of times they appeared in the "In Zone" area, **(I)** Total movement distance in the "In Zone" area, (**J**) Total distance moved, and (**K**) Mean velocity were measured. (**L**) Duration of complete descent in the pole test Symbols: Open triangle represents 2–3-month-old young mice; open circle indicates Old mice; closed rectangle symbolizes Treated Old mice. Each test began with 16–18 mice from each group *, **, ***: *p* values for comparison between Young and Old groups, * <0.05, ** <0.01, *** <0.001; §, §§, §§§: *p* values for comparison between Young and Treated (Trt-O) groups, § <0.05, §§ <0.01, §§§ <0.001; #, ##, ###: *p* values for comparison between Old and Trt-O groups, # <0.05, ## <0.01, ### <0.001

at six-week intervals. Experiments to track hpEVs using palm-tdTomato performed in vivo measurements 24 h after injection (according to the half-life of the tdTomato protein). Behavioral assays were conducted on the mice during the breaks between these injections. Depending on the treatment set, mice were euthanized either two weeks post the first injection or two weeks after the third, and various tissues were harvested for subsequent analyses. For in vitro studies, hpEVs were administered at a final concentration of 2 μg/mL. This dosage was selected based on our previously published study (Park et al., *Cells*, 2021), which demonstrated that placenta-derived EVs exhibited potent antiviral activity and promoted cell survival in a dose-dependent manner without cytotoxicity. In particular, EV concentrations ranging from 2.5 to 5 μg/mL resulted in full suppression of SARS-CoV-2 infection in Vero cells, while partial inhibition was observed at 1.25 μg/mL. Furthermore, the functional microRNA content of EVs at 1–2 μg was sufficient to mediate measurable biological effects. Therefore, the 2 μg/mL dose was selected as a biologically relevant and safe concentration for downstream in vitro assays.

Behavioral assessments

To evaluate the potential enhancement in functional behaviors of aged mice after hpMSC infusion, we carried out an array of behavioral tests. These assessments encompassed cognitive, locomotor, motor function, and exploratory behaviors, conducted in line with methodologies from previous research, albeit with certain modifications [10, 24]. Additional test procedures are elaborated upon in the Supplement Information.

Morris water maze (MWM) test

This test involved a 1.2-meter diameter pool with a hidden platform in one quadrant. Mice were given 60 s to locate the submerged platform, with training sessions over five days and a probe trial on the sixth day.

Locomotion test

Conducted in a 40 × 40 cm arena divided into two areas, mice were observed for 15 min as they moved freely.

Video monitoring

All behavioral tests, including the MWM, locomotion test, open field test, and elevated plus maze, were recorded using a CCD camera system connected to a computer and monitored with the EthoVision video-tracking system.

Pole test

To evaluate strength, coordination, and balance, mice were trained and tested on a 42.5 cm vertical pole, with their performance time recorded over several days.

Quantitative PCR analysis of hippocampal tissues and cells

Total RNAs were isolated from cells and hippocampal tissues using the TRIzol method (Invitrogen, Waltham, MA, USA) following the manufacturer's recommended protocol. A more detailed description of the procedure can be found in the Supplement Information. The PCR primers utilized in this study are listed in Supplement Table 6.

Transfection of plam-tdTomato

Palm-td lentivirus was obtained from Ph.D. Hwang at Seoul National University [25]. For transfection, hpMSCs were plated in a T-75 flask and treated with 800 μL of fabricated Palm-td lentivirus and 8.8 μL of polybrene (10 mg/mL, Santa Cruz Biotechnology). After 48 h, tdTomato fluorescence-positive cells were quantified using FACS analysis (Beckman Coulter, CA, USA).

Culture of HfNPCs

hfNPCs utilized in this study were sourced from spontaneously aborted human fetal brain tissue (8 ~ 14 gestational weeks) and cultured based on the methods previously detailed by Moon et al. [26]. A comprehensive description of the hfNPCs culture procedure can be found in the Supplement Information.

Coculture of HpMSCs with HfNPCs

For coculturing, a transwell system was employed. hfNPCs were seeded onto either 6- or 12-well plates and incubated overnight at 37 °C in a humidified environment with 5% CO_2, 92% N_2, and 3% O_2. The following day, the upper inserts, which either contained hpMSCs (with a 3.0-μm pore size; high density; BD Falcon, NJ, USA) or were devoid of any cells, were gently positioned over the wells containing the hfNPCs. Every two days, the hpMSCs were refreshed, and the coculture was maintained in the hfNPCs medium for a total of four days.

RNA sequencing analysis

RNA sequencing was performed using mouse brain tissue (GSE305309). Sequencing was performed at Theragen Bio (Seongnam-si, Korea) using Illumina 2000. We aligned the reads to the mouse reference genome (GRCm38) using TopHat [27]. The read counts were normalized to the fragments per kilobase of exon per million (FPKM). To investigate the biological function of differentially expressed genes (DEGs), GO term and KEGG pathway analyses were performed using the DAVID bioinformatics Resource [28]. Small RNA sequencing was performed using placental derived extracellular vesicles (GSE305310). Sequencing was performed at the Beijing Genomics Institution (BGI, Beijing, China) using BGISeq-500. The reads were aligned to the human reference genome (GRCh38) using subread aligner [29]. The

miRNA read counts were normalized to the count per million (CPM). mirDB was used to predict the binding sites for miRNAs [30].

Nanoparticle tracking analysis (NTA)

hpEVs, diluted in PBS, were analyzed using a ZetaView Nanoparticle Tracking Video Microscope (Particle Metrix, Inning, Germany). The analysis entailed three cycles, each scanning 11 cell positions and capturing 60 frames per position. The settings used were: autofocus for focus; a camera sensitivity of 80.0 for all samples; a shutter speed of 100; a scattering intensity of 1.2; and a cell temperature of 23℃. Videos captured were subsequently processed using the ZetaView Software 8.02.31, with set parameters: maximum particle size at 1,000 and minimum particle size at 5.

Transmission electron microscopy (TEM) imaging

5 µL samples of hpEVs, diluted to contain 0.5 µg protein, were placed onto hydrophilic grids. After allowing them to settle for a few minutes, the grids were rinsed with distilled water and subsequently contrasted for 20 s using 2% uranyl acetate. Imaging was then conducted with a JEM-1010 microscope (JEOL, Seoul, Korea) set to operate at 80 kV.

Western blot analysis

hpEVs and cells were lysed in 10 × RIPA buffer containing a protease inhibitor cocktail tablet (Roche, Basel, Switzerland) and phosphatase inhibitors Ⅱ and Ⅲ (Sigma-Aldrich, Mo, USA). An aliquot of each sample was subjected to 10% SDS-PAGE, followed by western blotting. Blots were blocked for 1 h in 10% skim milk. Antibodies specific for the following proteins were obtained from the indicated suppliers: CD81 (1:1,000, Santa Cruz Biotechnology, Dallas, TX, USA), CD9 (1:1,000, Santa Cruz Biotechnology), CD63 (1:1,000, Santa Cruz Biotechnology), TSG101 (1:500, Abcam, Cambridge, UK), Alix (1:500, Cell signaling technology, Danvers, MA, USA), Calnexin (1:1,000, Abcam), and Vinculin (1:2,000, Abcam). Primary antibodies were incubated with blots overnight at 4℃, followed by incubation with anti-rabbit or anti-mouse horseradish peroxidase (HRP) conjugated secondary antibodies (Jackson immunoresearch, West Grove, PA, USA) for 1 h. Immunoreactivity was detected using enhanced chemiluminescent HRP substrate (Merck Millipore, Darmstadt, Germany).

Labeling EVs with the lipophilic membrane dye PKH26 and detection of labelled EVs in FMD-NPCs

EVs were labeled using the PKH26 dye solution mix kit (Sigma-Aldrich), a red fluorescent cell linker designed for general cell membrane labeling, following the manufacturer's recommended protocol. Further details on the labeling procedure can be found in the Supplement Information.

Transfection of miRNAs into hfNPCs and EV-mediated delivery of Cy3-labeled miRNA mimic and imaging in hfNPCs

hfNPCs were seeded in 6-well plates at a concentration of 6×10^5/well. On the subsequent day, miRNAs, up to a concentration of 30 nM were transfected into the cells utilizing the Lipofectamine 3000 reagent as per the manufacturer's instructions (Invitrogen). The cells were then incubated with a mixture of the miRNA and reagent in complete hfNPC culture medium for 5 hours, after which the medium was refreshed. Following a further 48 to 96 h of incubation, both mRNAs and proteins were harvested from the transfected cells for subsequent analyses.

A 5′-Cy3–labeled synthetic miRNA mimic (non-targeting control sequence) was loaded into hpEVs with a commercial EV-loading reagent according to the manufacturer's protocol. Reactions were quenched and passed through qEV columns to remove free mimic; EV-containing fractions were pooled and concentrated with 100-kDa centrifugal filters. Loading controls included (i) hpEVs processed without mimic (unloaded hpEVs) and (ii) "mock-loaded" EVs processed identically without reagent. hfNPCs were plated on poly-D-lysine–coated coverslips (≥ 70% confluency), treated with hpEV–miRNA (equivalent to 2 µg EV protein/mL) for 6–24 h, washed with PBS, fixed in 4% paraformaldehyde, counterstained with DAPI, and imaged by fluorescence/confocal microscopy under identical exposure settings. A lipofection positive control was prepared by delivering the same Cy3-mimic with Lipofectamine per the manufacturer's instructions.

EV-Mediated transfer of plasmids containing GFP or OCT4 and SOX2 genes via CPP complex

To facilitate the transfer of plasmids housing the *GFP* or *OCT4* and *SOX2* genes into target cells, a cell-penetrating peptide (CPP) complex was employed. This complex was created by fusing a DNA-binding peptide with a cell-penetrating sequence. Initially, plasmids were combined with the CPP at a ratio of 3:1, involving 0.21 µg of the plasmids and 0.07 µg of CPP. A variant of CPP, devoid of the DNA-binding peptide, acted as a control. This blend was left undisturbed for an hour at room temperature. Subsequently, EVs, amounting to 0.14 µg, were mixed with the DNA-CPP concoction (totaling 0.28 µg) at a 1:2 proportion, and the resulting mixture was incubated for another 4 h at ambient temperature. This EV-DNA-CPP complex was then introduced to 1 ml of cell culture medium per well (1×10^5 cells/well of a 24-well plate). After incubating for 48 to 96 h, either total RNA was extracted, or fluorescence imaging analyses were executed.

Neurosphere formation assay

Neurosphere formation assay was conducted using old hfNPCs cultured under non-adherent suspension conditions. Cells at passages 23 and 25 were dissociated into single cells and seeded at a concentration of $3 \times 10^3/cm^2$ onto non-coated, low-attachment plates with serum-free medium supplemented with epidermal growth factor (EGF) and basic fibroblast growth factor (bFGF). Both untreated control and 2 μg/ml hpEV-treated groups were prepared at the time of cell seeding. Cultures were maintained at 37 °C with 5% CO_2 for 3 to 5 days to allow neurosphere formation. Representative images were acquired on Day 3 for passage 23 and Day 5 for passage 25, with scale bars of 500 μm. Neurosphere numbers were quantified manually from three independent experiments. Statistical analysis was performed comparing neurosphere numbers between control and hpEV-treated groups.

Assessment of BBB permeability and brain parenchymal EV penetration

To evaluate age-related differences in blood–brain barrier (BBB) permeability and confirm the penetration of systemically administered hpEVs into the brain parenchyma, we performed an Evans Blue tracer assay in young (2.5-month-old) and aged (21-month-old) C57BL/6J mice. Evans Blue (2% w/v in PBS; 4 mL/kg body weight) was administered via the tail vein under brief isoflurane anesthesia. One hour post-injection, mice were deeply anesthetized and perfused transcardially with ice-cold PBS to remove intravascular dye. Brains were dissected and examined both intact and as 1 mm coronal sections for gross visualization of dye distribution. In parallel, a subset of mice received intravenous palm-tdTomato-labeled hpEVs or hpMSC-derived EVs 24 h prior to tracer injection to enable co-localization analysis. Evans Blue fluorescence (albumin-bound) and tdTomato signals were assessed in fresh sections using a fluorescence stereomicroscope (Leica M205 FA) and confocal microscopy (Zeiss LSM 880). Dye accumulation beyond vascular boundaries into the parenchyma was taken as evidence of BBB disruption. Aged mice exhibited robust Evans Blue extravasation and EV fluorescence within brain parenchyma, whereas young mice displayed minimal tracer or EV penetration beyond the vasculature. Representative images are shown in Supplementary Fig. S2C.

Statistical analysis

All statistical evaluations were performed using IBM SPSS Statistics version 20.0 (IBM SPSS; IBM SPSS Korea, Inc., Seoul, Korea). The viability, image intensity data, and all in vitro results were subjected to various statistical tests, including the Kaplan-Meier Estimation and log-rank test. Depending on the data distribution, either the two-sample t-test (or its non-parametric counterpart, the Wilcoxon rank sum test) or the one-way ANOVA (or its non-parametric alternative, the Kruskal-Wallis test) was used. Where applicable, post hoc analyses were carried out using Fisher's least significant difference, with adjustments for multiple comparisons through the Bonferroni procedure. For datasets involving repeated measures or nested data structures, a linear mixed model was employed, incorporating random effects to account for variability among mice. The post hoc test used for the linear mixed model was Fisher's least significant difference.

Results

Multiple systemic injections of HpMSCs improved survival rate of aged mice

To investigate the potential of stem cells to modulate normal, non-pathological aging, we repeatedly infused hpMSCs into mice of 18–19 months ("Treated Old" group: Trt-O) through the tail vein (Fig. 1A). Age-matched control mice ("Old" group) were treated with phosphate-buffered saline (PBS) according to the same schedule. The Old mice gradually died, and less than half of them survived for 175 days after the first injection. In contrast, three-quarters of the Treated Old mice were alive during the same period and remained viable for up to 7 months (Fig. 1B), indicating that the infused stem cells had no detrimental effects and were beneficial for the mice's survival.

HpMSCs treated aged mice exhibited enhanced cognitive functions

In our study using Morris Water Maze (MWM) assays, we observed that aged mice treated with hpMSCs showed significant improvements in cognitive and memory functions. Initially, both Old and Treated Old mice took longer to locate a platform compared to young mice (Fig. 1C). However, after the third treatment, the Treated Old mice reached the platform as quickly as the young group, unlike their untreated counterparts. They also passed through the platform area more frequently (Fig. 1D) and spent a similar amount of time in the target zone (Zone 1) as young mice, indicating enhanced memory retention (Fig. 1E). Nonetheless, the similar total movement distance and mean velocity between the Treated Old and Old groups indicate that hpMSCs enhanced cognitive and spatial memory functions (Fig. 1F and G). In terms of locomotive activity, the Treated Old mice demonstrated a significant increase in movement within the target zone after the third injection (Fig. 1H and I), contrasting with old mice who moved more in non-target areas (Fig. 1J and K). Furthermore, in a pole test, the Treated Old mice's descent speed matched that of the young mice after repeated treatments (Fig. 1L). These findings collectively show that multiple

infusions of hpMSCs effectively ameliorated age-related declines in cognitive, memory, and locomotive functions, with notable improvements after the third infusion.

HpMSCs downregulated age-related and antioxidant genes in the age mice

Given that hpMSC treatment curtails the aging-associated decline in spatial memory and cognition, we sought to examine whether hpMSCs alter the expression of age-related genes in the hippocampus. We found that expression of $p16^{INK4a}$, a representative aging marker, was induced in the aged mice but was significantly suppressed in Treated Old mice compared to that in the Old group (Fig. 2A). Induced expression of High Mobility Group AT-Hook 2a (*HMGA2a)*, which is involved in senescence associated heterochromatin foci formation [31], in the Old group was reduced in the Treated Old to the comparable level in the Young group (Fig. 2B). Expression of Glial Fibrillary Acidic Protein (*GFAP)*, an astrocyte marker and a potential indicator of age-related changes in neuroinflammation and cognitive function [32], was substantially higher in the Old group compared to that in Young mice. However, an increase in *GFAP* expression was significantly abated in the Treated Old group, indicating that hpMSCs can repress the astrocyte-associated immune aging in aged brain (Fig. 2C). The expression of antioxidant genes was examined because an increase in oxidative stress drives hippocampal aging [33]. The key antioxidant genes, Superoxide Dismutase 2 (*SOD2*) and Catalase (*CAT*), but not Superoxide Dismutase 1 (*SOD1)*, significantly increased in the Old group and the hpMSC treatment nullified the upregulation of them, bringing down to the level detected in Young mice, suggesting that the cell treatment protects the hippocampus against the increased oxidative stress mediated damage in aged mice (Fig. 2D-F).

Initially, we verified the cellular aging process of neural stem/progenitor cells. We observed a consistent decline in the proliferation of hfNPCs from passage 22 (Fig. S1A), which was associated with a diminished expression of Proliferating Cell Nuclear Antigen (*PCNA)* and a heightened expression of $p16^{INK4a}$ (Fig. S1B). Concurrently, there was an enlargement in cell size and a greater diversity within the cell population (Fig.S1C). We observed a decrease in PCNA and an increase in $P16^{INK4a}$, correlating with a gradual decline in cellular

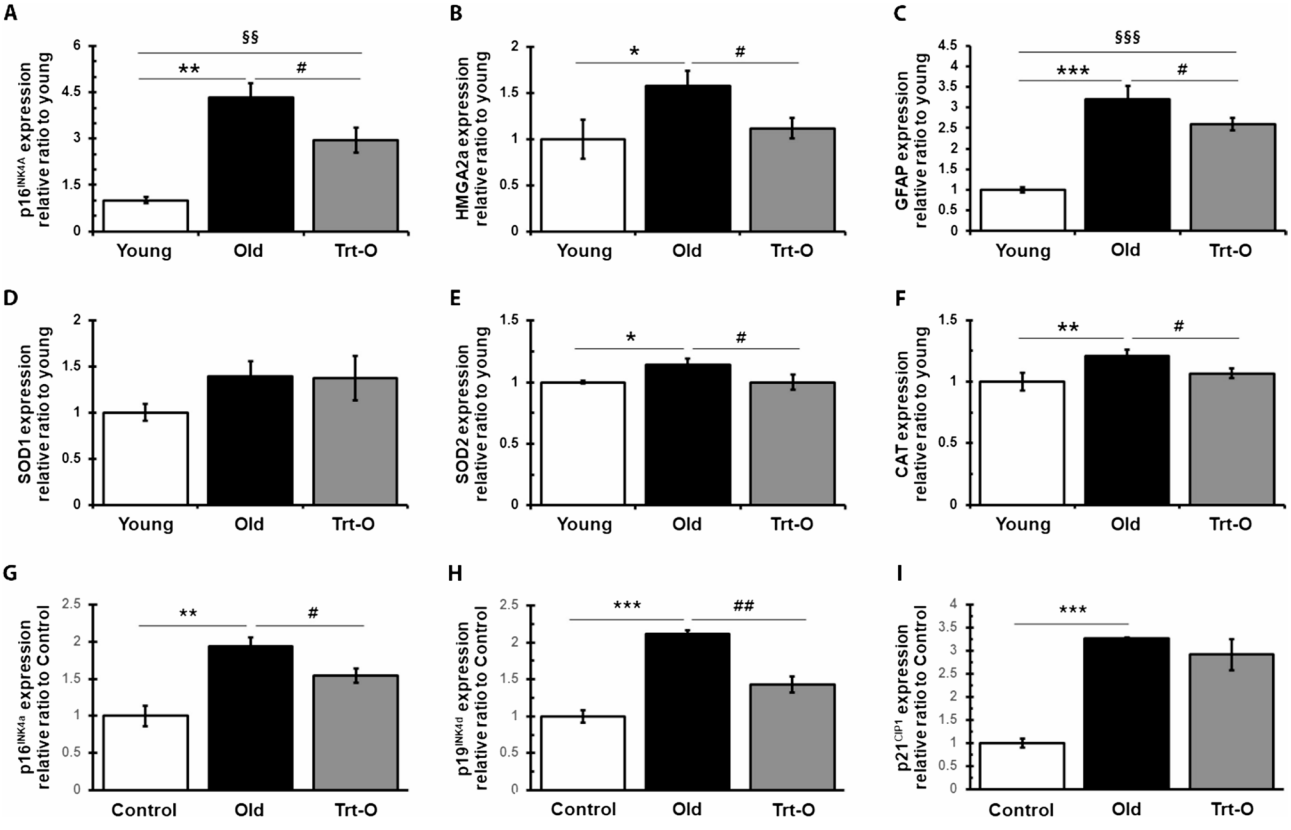

Fig. 2 hpMSC Suppresses Expression of Aging and Oxidative Stress-Related Genes in Hippocampi of Infused Aged Mice and in Co-Cultured hfNPCs. hpMSC-mediated modulation of the expression of (**A-C**) aging-related genes, $p16^{INK4a}$, *HMGA2a*, and *GFAP*, (**D-F**) antioxidant genes, *SOD1*, *SOD2*, and *CAT* in aged mice, and (**G-I**) senescence associated genes, $p16^{INK4a}$, $p19^{INK4d}$, and $p21^{CIP1}$, in co-cultured older hfNPCs, Trt-O *, **, ***: *p* values for comparison between Young and Old groups, * <0.05, ** <0.01, *** <0.001; §, §§, §§§: *p* values for comparison between Young and Treated (Trt-O) groups, § <0.05, §§ <0.01, §§§ <0.001; #, ##, ###: *p* values for comparison between Old and Trt-O groups, # <0.05, ## <0.01, ### <0.001

proliferation capacity, indicating cellular senescence. Additionally, hfNPCs, essential for tissue regeneration and maintenance, exhibit reduced proliferative and differentiation capabilities with aging. To evaluate this, we induced neuronal differentiation and analyzed class III β-tubulin (*TUJ-1*) expression levels. In hfNPCs induced to undergo spontaneous differentiation at passage 25, TUJ-1 expression was significantly reduced compared to passage 17. The results showed a decrease in TUJ-1 levels with increasing cell passages, indicating diminished differentiation capacity and increased cellular senescence. This highlights the strong association between cellular senescence and the decline in both proliferation and differentiation abilities, demonstrating aging neural cells with functional impairments and challenges in tissue regeneration (Fig. S1D).

Because the infused hpMSCs profoundly influenced the gene expression and functions of brain in the treated mice under their limited capability to cross blood-brain barrier (BBB), we proceeded to coculture either control hfNPCs or older cells on a plate with hpMSCs positioning in the upper chamber of a trans-well setup, which allowed us to scrutinize the potential of hpMSCs in mitigating cellular senescence in a paracrine dependent manner. Compared to the control, we observed a significant increase in the expression of senescence markers $p16^{INK4a}$, $p19^{INK4d}$, and $p21^{CIP1}$ in aged hfNPCs. Interestingly, the co-culture with hpMSCs notably downregulated the levels of $p16^{INK4a}$, $p19^{INK4d}$, and $p21^{CIP1}$, although the decrease in $p21^{CIP1}$ was not statistically significant compared to its increased levels in aged hfNPCs. This indicates that hpMSC treatment has the senescence of hfNPCs. (Fig. 2G-I). Together, these results suggest that the infused cells counter brain aging processes and shield hippocampal neurons and other brain cells by activating specific pathways, such as reducing oxidative stress and other aging-related stresses, thereby enhancing, or sustaining cognitive function.

The RNA-seq analysis revealed that neural functions and signals

To gain an insight into how hpMSCs contribute to regenerative effects, we conducted Gene Ontology (GO) term analysis with the total mRNAs isolated from the hippocampi of Young, Old, and Treated Old. Compared to Young, the significant changes in the aged hippocampus were identified in biological activities, especially immune/inflammation involved functions and neuronal activity-related extracellular signals and endocytosis (Table S1). In addition, analysis of differentially expressed genes (DEGs) in the hippocampi of the Old group showed inhibition of synaptic activity and signaling-related genes, while genes related to various diseases, including neurodegenerative and inflammatory diseases, were activated, indicating a functional decline with increased neuronal pathogenesis in the Old group (Table S2). When compared to the Old group, GO terms with bigger than 1.5-fold change in the Treated Old group included positive regulators of proliferation, brain development, biosynthesis, and metabolism, suggesting that the infusion of hpMSCs modulated the expression of various genes associated with anti-aging processes (Table S3). Focusing on brain functions, we found that hpMSCs treatment strongly affected genes related to synaptic activity and transmission, such as nerve impulses, synaptic transmission, neurotransmitter secretion, ion transport, and cell-to-cell signaling (Table 1). These results were consistent with DEG analysis of Old and treated Old mice, presenting that hpMSC treatment enhanced several neuronal signaling pathways, including calcium signaling, salivary secretion, serotonergic synapses, and amphetamine addiction, while inhibiting neuroactive ligand-receptor interaction signaling pathways (Table 2). The observed enhancements in neuronal activities and locomotion may be attributed to hpMSCs-induced upregulation of calcium signaling genes and amphetamine response genes [34]. The DEG analysis supported

Table 1 Changes in Brain-Associated gene ontology terms in hpMSC-Treated old mice compared to old mice

Term	Count	*P* Value
Transmission of nerve impulse	42	2.867E-09
Cell–cell signaling	49	3.093E-09
Synaptic transmission	36	4.782E-09
Neurotransmitter transport	22	3.312E-08
Ion transport	85	1.253E-07
Metal ion transport	60	1.756E-07
Neurotransmitter secretion	14	2.395E-07
Intracellular signaling cascade	100	5.914E-07
Neuron differentiation	54	8.752E-07
Neuroactive ligand–receptor interaction	39	1.323E-06
Regulation of neurotransmitter levels	17	1.825E-06
Potassium ion transport	29	1.954E-06
Cation transport	62	6.291E-06
Cell adhesion	66	6.507E-06
Biological adhesion	66	6.898E-06
Generation of a signal involved in cell–cell signaling	19	7.503E-06
Cell projection organization	43	1.487E-05
Behavior	50	3E-05
Calcium signaling pathway	29	3.299E-05

Table 2 Changes in Brain-Associated KEGG pathways in hpMSC-Treated old mice compared to old mice

Signaling pathways	Status
Neuroactive ligand–receptor interaction	Inhibited
Calcium signaling pathway	Activated
Salivary secretion	Activated
Serotonergic synapse	Activated
Amphetamine addiction	Activated

that the hpMSCs could restore the biological deterioration such as decline of salivary function, a characteristic of aging in both humans and rodents, via induction of salivary secretion-related genes [35]. We also compared known aging genes with our DEG analysis and categorized the upregulated and downregulated genes in each signaling pathway (Table S4). Our findings indicate that hpMSCs upregulated positive regulatory genes linked to learning and neuronal activity, such as the GRIN family, SYNJ1, SYNGAP1, RELN, and TBR1, consistent with Table S3.

EVs from hpMSCs, hpEVs, suppressed cellular senescence of HfNPCs

Given the capacity of EVs to cross the BBB and to attenuate brain aging potentially through the modulation of miRNAs within them, it is evident that hpEVs, EVs derived from hpMSCs, stand as pivotal key factors in rejuvenating and delaying brain aging. To explore the potential influence of hpEVs in blunting brain aging processes, the hpEVs isolate from hpMSC culture media were characterized first. Nanoparticle tracking analysis (NTA) on the hpEVs showed a total concentration of approximately 9.7 × 1010 particles/ml, with a mean diameter of 148.5 nm and a size distribution between 100 and 200 nm, indicating that the majority of hpEVs were distinct from other types of microvesicles or apoptotic bodies (Fig. 3A). The morphological and molecular attributes of the hpEVs were analyzed to evaluate their potential utility. Transmission electron microscopy (TEM) demonstrates that the hpEVs presented a rounded membrane morphology with a consistent size, around 200 nm in diameter, aligning with the findings from the NTA (Fig. 3B). Furthermore, the western blot analysis confirmed the presence of typical EV surface markers in the hpEVs, such as the tetraspanins CD9, CD63, and CD81, as well as other markers Alix, and TSG101, using Vinculin as a control (Fig. 3C). A slight presence of Calnexin, an endoplasmic reticulum (ER) protein, indicated minimal contamination with ER-derived vesicles.

Next, to assess the potentials of hpEVs to influence neuronal cellular senescence, we treated older hfNPCs with hpEVs (2 μg/ml) for four days and then analyzed alteration of gene expression linked with cellular senescence and oxidative stress. Our analysis revealed a decrease in expression of several senescence related genes, p19INK4d, p21CIP1, and p53 in the hpEV treated older hfNPCs although no change was observed in the expression of p16INK4a (Fig. 3D), indicating that hpEVs have the capability to suppress a subset of genes related to senescence. In additions, the expression of antioxidant genes was also influenced by hpEVs treatment (Fig. 3E): both SOD1 and SOD2, and CAT genes were induced along with increased expression of Nuclear Factor Erythroid 2-Related Factor 2 (NRF2), a transcription factor for antioxidant gene, after the four-day treatment, suggesting that the hpEVs can modulate the NRF2-antioxdant gene signaling axis and protect the cells against the oxidative stress implicated damages.

To investigate whether hpEVs attach to the cell membrane of hfNPCs and deliver their internal cargo to exert anti-aging effects, we conducted a further experiment. The results demonstrated that hpEVs effectively attach to and remain on the surface of hfNPCs. After labeling hpEVs with PKH26 and treating hfNPCs with these labeled hpEVs for 24 h, fluorescence microscopy revealed that the PKH26-labeled hpEVs were prominently detectable on the cell membrane of hfNPCs, indicating successful attachment. This adherence suggests that hpEVs can potentially deliver their anti-aging cargo to hfNPCs. Additionally, visualization of the hfNPC cytoplasm using a Nestin antibody confirmed the colocalization of hpEVs on the hfNPC membrane, further supporting their potential role in anti-aging interventions. Furthermore, we utilized fluorescent EV reporters, specifically palmitoylated-tdTomato (palm-tdTomato), to verify that EVs released from intravascularly injected hpMSCs migrate to the brain. By transfecting hpMSCs with palm-tdTomato via a lentivirus vector, tdTomato proteins were tagged to the cell membranes, enabling the detection of tdTomato-labeled EVs released from these cells [36]. As shown in Fig. S2A, fluorescence signals confirmed the presence of tdTomato in the cell membranes of hpMSCs transfected with the palm-tdTomato lentivirus. We then intravascularly injected these transfected cells into 18-month-old aging mice and examined their brains using confocal microscopy. The results were striking: tdTomato + EVs were detected in the mouse brains, with co-localization of the exosomal marker CD63 (Fig. 3G). *To further obtain direct evidence of functional miRNA transfer from hpEVs into recipient cells, we performed a fluorescent gain-of-signal delivery assay using hpEVs loaded with a 5′-Cy3–labeled synthetic miRNA mimic. After removal of unincorporated mimic, hfNPCs were exposed to hpEV–miRNA and imaged. As shown in Supplementary Fig. S4, cells treated with hpEV–miRNA displayed robust punctate Cy3 signal within the cytoplasm, whereas unloaded hpEVs produced no detectable Cy3 signal. A lipofection positive control exhibited the expected intracellular Cy3, and the hpEV–miRNA condition showed comparable or greater mean fluorescence intensity across fields. Quantitative single-cell analysis confirmed significantly higher Cy3 intensity in the hpEV–miRNA group versus controls, indicating efficient EV-mediated delivery of miRNA cargo into hfNPCs. These uptake data complement our transcriptomic findings following hpEV exposure and support the biological relevance of abundant hpEV miRNAs in modulating targets in hfNPCs.*

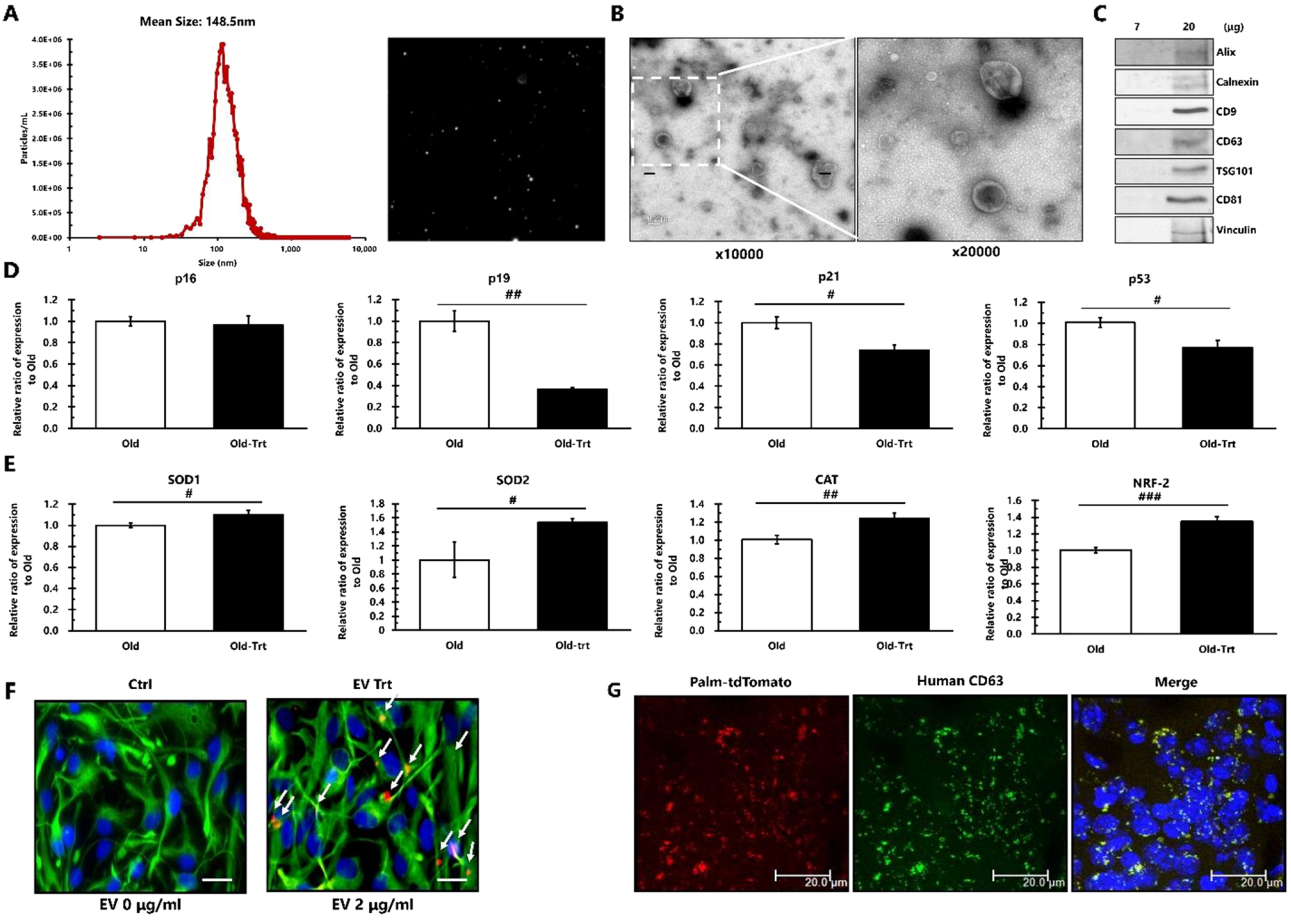

Fig. 3 Characterization of Human Placenta-derived Extracellular Vesicles (hpEVs) Isolated from Conditioned Media of hpMSCs. (**A**) Nanoparticle Tracking Analysis (NTA) of the hpEVs samples showed a representative particle size distribution plot derived from sample measurements. (**B**) Transmission Electron Microscopy (TEM) images of the hpEVs are displayed on the left, with a magnified view of the designated square region. The respective scale bars measure 200 nm and 100 nm, respectively. (**C**) Western blotting analysis revealed specific markers on a representative membrane image. The expression of EV markers such as *CD9*, *CD63*, *CD81*, *TSG101*, and *Alix*, as well as *Vinculin* and the endoplasmic reticulum protein *Calnexin* in the hpEVs, was evident. (**D**) Exposure to hpEVs (at 2 μg/ml) modulated a subset of genes associated with senescence in the older hfNPCs. **(E)** Expression of oxidative stress and stress responsive genes in old NPCs was induced in response to the hpEV treatment. **(F)** After a 24-hour treatment with 2 μg of PKH26-labeled hpEVs, hfNPCs were subjected to immunocytochemistry staining. The cells were distinctly stained with DAPI (blue), *Nestin* (green), and PKH26 (red). The combined images are also presented. The scale bar represents 100 μm. **(G)** Representative confocal images of the mouse brain treated with palm-tdTomato-hpMSCs administered via intravascular injection. Evidence of EVs migration to the brain is shown by the detection of tdTomato (red) and human CD63 (green). Scale bars are 100 μm. #, ##, ###: *p* values for comparison between Old and Old-Trt groups, # <0.05, ## <0.01, ### <0.001

This provides compelling evidence that hpMSC-derived EVs can traverse the vascular system and deliver their cargo to the brain, highlighting their potential for targeted anti-aging therapies. Interestingly, we did not observe this phenomenon in young mice. As shown in Fig. S2B, hpMSC-derived EVs were not observed in the brains of Young mouse that received hpMSC administration. This difference indicates that hpMSC-derived EVs can traverse the compromised BBB in Old mouse, allowing them to reach and exert effects in the brain. This phenomenon was not observed in Young mouse with an intact BBB. Taken together, these results suggest that hpEVs play a crucial role in mediating the anti-aging effects of hpMSCs. They achieve this by transferring their cargo and modulating a subset of genes involved in replication-associated cellular senescence, as well as genes regulating oxidative stress and redox status. This highlights the potential of hpEVs as a therapeutic tool for targeting age-related conditions and improving brain health in aging populations.

miRNA-enriched HpEVs modulated neuroinflammation- and TLR4-associated signaling pathways

EVs function as cellular couriers, facilitating intercellular communication by transferring a variety of cargos to both adjacent and remote cells [16]. Among cargos, miRNAs can orchestrate key aging processes such as cellular senescence and stem cell depletion by regulating gene expression post-transcriptionally [37, 38]. To gain mechanistic insight into the anti-aging effects facilitated by

miRNAs in hpEVs, we performed small RNA sequencing analysis with total RNAs from hpEVs. This analysis pinpointed 18 predominant human miRNAs, hsa-miRNAs, each of which accounts for more than 1% of the total miRNA pool and collectively represent 80% of all identified miRNAs (Fig. 4A). The GO analysis highlighted that these predominant miRNAs play a critical role in modulating a variety of processes intricately linked to aging, such as cellular senescence, brain functionality, and both acute and chronic inflammatory responses. They also influence the dynamics of Toll-Like Receptor (TLR) signaling pathways, NFκB signaling networks, and amyloid precursor protein (APP) processes (Fig. 4B). Specifically, we focused our analysis on the TLR4 pathway, given its heightened expression levels in the aging brain and significant association with the majorly abundant miRNAs targeting TLR4 signals [39]. Notably, hsa-miR-92a-3p, the miRNAs of the highest abundance, and hsa-miR-21-5p directly target TLR4. Additionally, hsa-miR-122-5p is involved in modulating RB binding protein 5 (RBBP5) and CD40L, and hsa-miR-150-5p interacts with a mRNA coding TLR4 interactor with leucine-rich repeats (TRIL). Furthermore, hsa-miR-22-3p has been identified as a regulator of a NOD-like receptor family, pyrin domain containing 3 (NLRP3) and a p53 pathway showing a comprehensive influence on a range of aging-related processes and signaling pathways [39, 40]. Remarkably, recent studies have identified that the TLR4 and NLRP3 inflammasome pathways play a critical role in inducing cellular senescence and preventing the development of cancer stem cells in brain by suppressing the activity of pluripotent transcription factors (PTFs) such as OCT4, SOX2, KLF4, and C-MYC (OSKM) [41, 42].

Drawing upon recent findings, we sought to further scrutinize the role of key miRNAs associated with TLR4 within hpEVs, with a central focus on SOX2, one of the most PTFs in brain. First, we observed remarkable increase in TLR4 expression in old hfNPCs compared to that in young cells (CONT), which was significantly reversed in the hpEV treated old cells (Fig. 4C), indicating that certain miRNAs harbor the potential to fine-tune TLR4 expression. To further elucidate the roles of miRNAs in the hpEV associated modulation of TLR4 expression, we transfected the older hfNPCs with synthetic

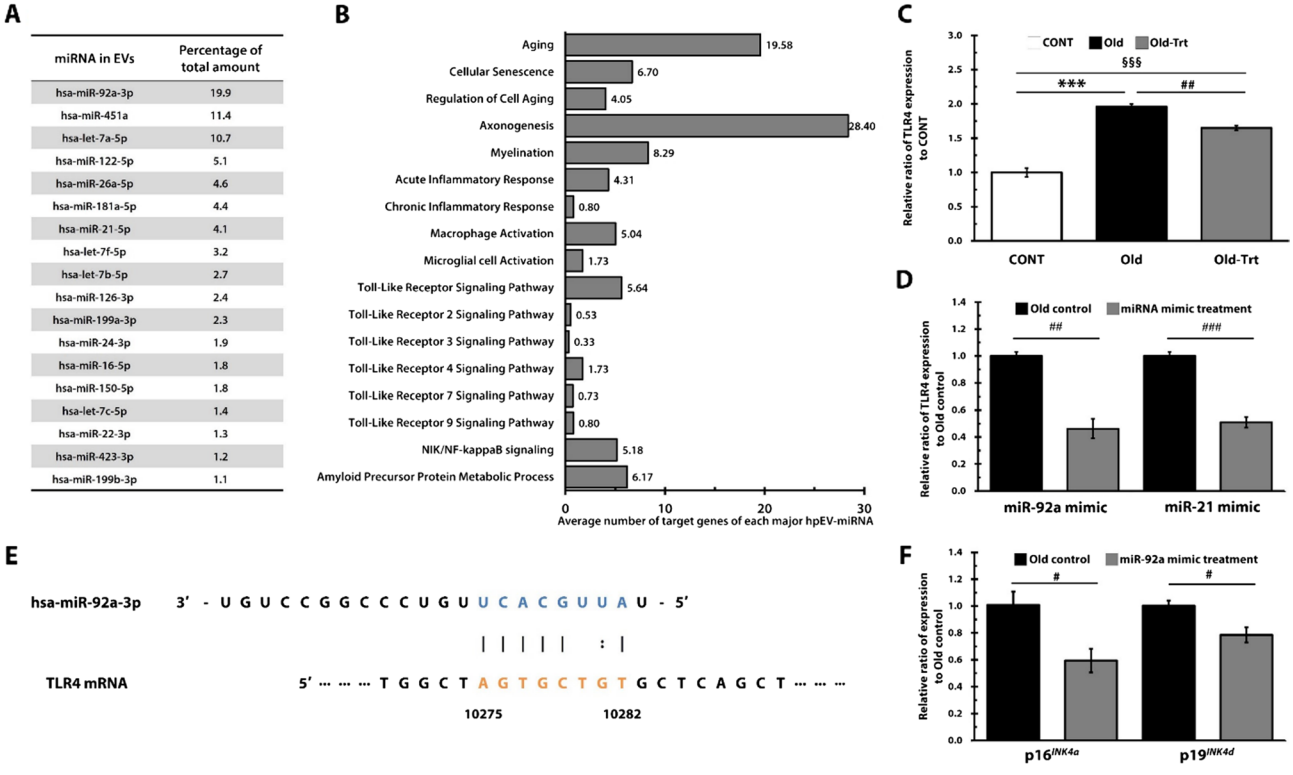

Fig. 4 MicroRNA Analysis in EVs and Regulation of Toll-like Receptor 4 (TLR4) by miRNAs. **(A)** Predominant miRNAs present in hpEVs. Listed are the miRNAs that constitute more than 1% of the total content. (**B**) Analysis of aging-, inflammation-, and brain function-related GO terms in relation to miRNAs in hpEVs. The numbers indicate the average count of genes each miRNA targets within the pathways. (**C**) *TLR4* expression is elevated in old hfNPCs but is suppressed with hpEV treatment. (**D**) The miRNA mimics targeting *TLR4* efficiently downregulated the *TLR4* expression in old hfNPCs (**E**) The hsa-miR-92a-3p binds the target *TLR4* mRNA. A line means a perfect match, and a dot line means G: U wobble pairs. An empty space in seed regions means mismatch. (**F**) The miR-92a mimic significantly repressed the expression of senescence associated genes, $p16^{INK4a}$ and $p19^{INK4d}$ in old hfNPCs *, **, ***: *p* values for comparison between Control and Old groups, * <0.05, ** <0.01, *** <0.001; §, §§, §§§: *p* values for comparison between Young and Treated (Trt-O) groups, § <0.05, §§ <0.01, §§§ <0.001; #, ##, ###: *p* values for comparison between Old and Treated (Old-Trt) groups, # <0.05, ## <0.01, ### <0.001

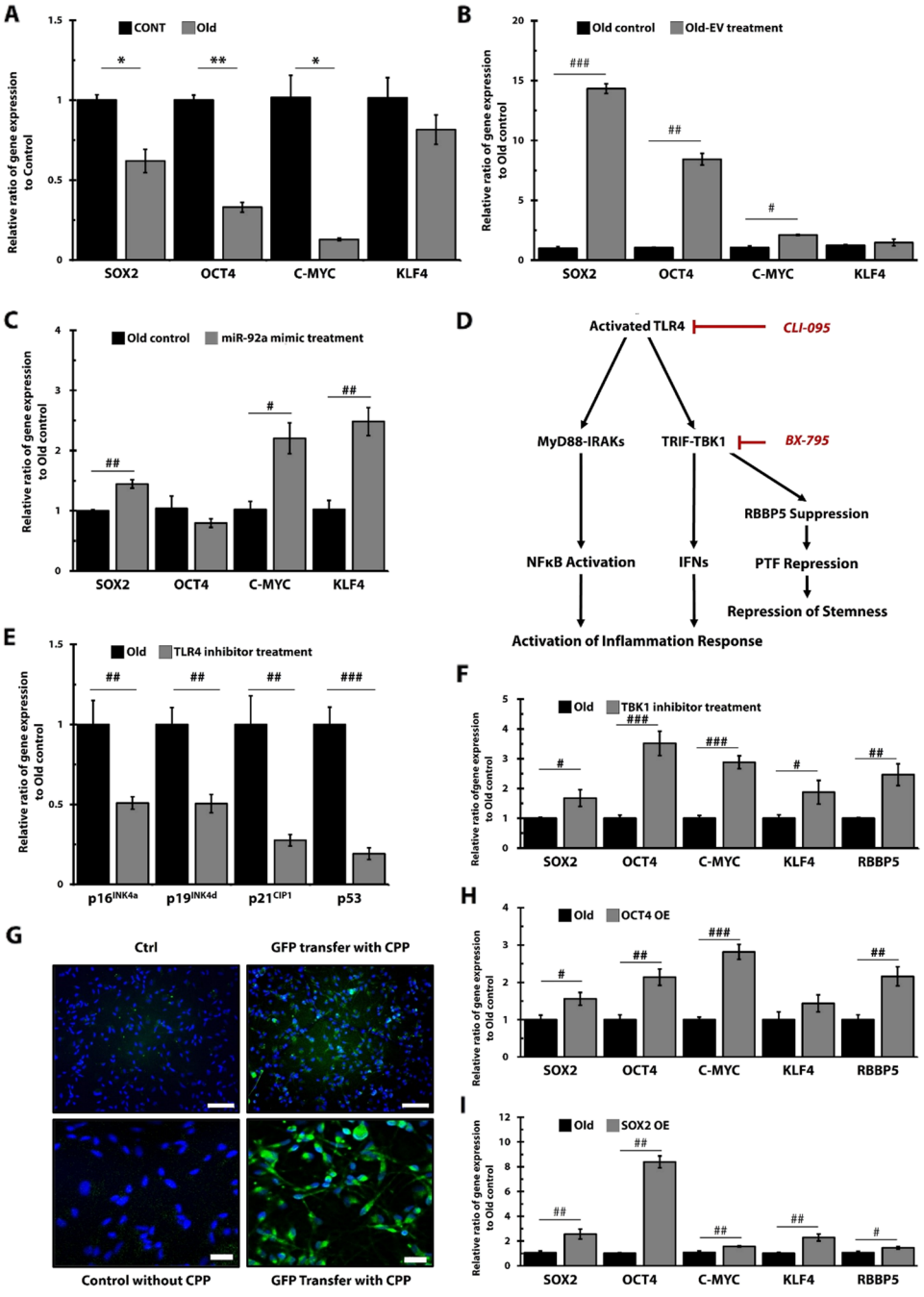

Fig. 5 (See legend on next page.)

miRNA mimics targeting TLR4 - specifically the mimics for hsa-miR-92a-3p and hsa-miR-21-5p in hpEVs. Both miRNA mimics were notably potent in inhibiting TLR4 expression, with the miR-92a mimic demonstrating the most pronounced downregulation effect, reducing expression levels by approximately 56%. This finding strongly suggests that TLR4 is a prominent target gene of miRNAs present within hpEVs (Fig. 4D). The computational analysis revealed that hsa-miR-92a-3p could potentially and strongly bind to the 10,275 ~ 10,282 region of the TLR4 gene. This binding is characterized by a microRNA-target hybridization energy (or Gibbs free energy of the duplex, dG) of −18.1. A more negative duplex dG value, like the one observed here, indicates a more stable and possibly more effective regulatory binding between the miRNA and its target, suggesting a higher affinity between the miR-92a mimic and the TLR4 gene region specified. Moreover, the analysis showed a combined interaction energy of −9.74 ddG (delta delta G), a parameter that indicates the change in stability of

(See figure on previous page.)

Fig. 5 hpEVs Mitigate Cellular Senescence of hfNPCs by Modulating the TLR4-mediated Transcriptional Repression of Pluripotent Transcription Factors (PTF), OSKM. (**A**) Decreased expression of OSKM in hfNPCs in the old hfNPCs. (**B**) hpEV treatment induced *SOX2*, *OCT4*, *and C-MYC* expression in the old hfNPCs. (**C**) The *TLR4*-targeting miR-92a mimic treatment enhances the expression of *SOX2*, *C-MYC*, and *KLF4*. (**D**) A concise diagram depicting *TLR4* signaling. *TLR4* activation triggers two distinct downstream signaling pathways: MyD88-IRAKs and TRIF-TBK1. The recruited MyD88-IRAKs complex activates *NFκB*, leading to inflammation and aging. Similarly, TRIF-TBK1 induces inflammation by activating interferon response elements. Furthermore, TRIF-TBK1 undermines the stemness of numerous stem cells by inhibiting RBBP5-mediated induction of PTFs. Key terms: MyD88 refers to myeloid differentiation primary response protein 88; IRAKs stand for interleukin 1 (IL-1) receptor-associated kinases; *NFκB* is nuclear factor κB; TRIF denotes TIR domain-containing adaptor protein-inducing interferon-β; TBK1 is TANK binding kinase 1; and *RBBP5* represents retinoblastoma binding protein 5. **(E)** The *TLR4* inhibitor CLI-095 (2 μM) suppressed the expression of senescence-related genes in old hfNPCs after 48 h of treatment. **(F)** Treatment with a *TBK1* inhibitor, BX-795 (100 nM), for 48 h induced the expression of OSKM and *RBBP5* in old hfNPCs. **(G)** The hpEVs harboring *GFP* plasmids by the cell penetrating peptide (CPP) complexes were incubated with the hfNPCs for 96 h and the fluorescent microscopic images were acquired (upper lane). The Figures on the lower lane represent images from Confocal microscope. The cells were staining with DAPI (blue) and the pictures were merged with DAPI staining and *GFP* expression. Scale bar = 50 and 20 μm, fluorescent microscope and Confocal microscope, respectively. **(H)** Expression of transferred *OCT4* for 96 h induced the expression of *SOX2*, *OCT4*, *C-MYC*, and *RBBP5*. **(I)** Expression of transferred *SOX2* for 96 h induced the expression of OSKM and *RBBP5*. Note: CPP-assisted EV loading in panels (G–I) was performed as a proof-of-concept to assess the delivery capacity of hpEVs. This approach is distinct from the native hpEV mechanism studied in earlier experiments and was not intended to model physiological miRNA/mRNA transfer Data are presented as mean ± SD. *, **, ***: *p* values for comparison between Control and Old groups, * <0.05, ** <0.01, ***; #, ##, ###: *p* values for comparison between Old and Treated groups, # <0.05, ## <0.01, ### <0.001

the RNA-RNA interaction when a mutation occurs, further emphasizing the affinity and potential regulatory efficacy of hsa-miR-92a-3p with the specified region of the TLR4 gene (Fig. 4E). Consistent with these computational predictions, the inhibition of cellular senescence by the miR-92a mimic was corroborated by the observed downregulation of p16INK4a and p19INK4d expression in the mimic treated hfNPCs (Fig. 4F). Consequently, it can be inferred that hpEVs have the potential to delay or inhibit the senescence of hfNPCs through miRNA-mediated suppression of the TLR4 pathway.

HpEVs reactivation OSKM by the TLR4-targeting MiRNA expression

Building upon the insight from the relationship between *TLR4* and miR92a-3p in hpEVs, we subsequently examined the expression levels of OSKM in aging hfNPCs. Compared to CONT, the expression of *SOX2*, *OCT4*, and *C-MYC* significantly decreased in old hfNPCs, suggesting a diminished stem cell characteristic with advancing age (Fig. 5A). However, *KLF4* expression remained relatively stable, possibly because of its inherently low baseline expression as indicated by its CT values. When these aged cells were exposed to hpEVs, there was a pronounced upswing in the expression of *SOX2*, *OCT4*, *and C-MYC* (Fig. 5B). To evaluate the effects of hpEVs on cellular rejuvenation of hfNPCs, we treated late-passage old hfNPCs (p23) with hpEVs and assessed neurosphere formation. Compared with the control group, which displayed the aging-associated phenotype of strong adhesion and flattened growth, hpEV-treated cells showed a significant increase in suspension growth and neurosphere formation (Fig. 6A and B). In more senescent hfNPCs (p25), control cells failed to form neurospheres and predominantly exhibited adherent growth, whereas hpEV-treated cells retained the capacity to form neurospheres (Fig. 6C). These findings indicate that hpEV treatment alleviates the aging-induced adhesion phenotype of old hfNPCs and promotes restoration of stemness or maintenance of an undifferentiated state, thereby exerting cellular rejuvenation effects. This outcome, albeit somewhat anticipated, underscores that hpEVs mainly enhance the expression of *SOX2* among OSKM in NPCs, demonstrating the integral role of *SOX2* as an essential transcription factor for maintaining pluripotency and orchestrating neural differentiation [43], and the heightened sensitivity of the *SOX2* signaling pathway to hpEVs in NPCs. To further investigate the interplay between hsa-miR-92a-3p and *TLR4* expression and its potential impact on OSKM expression, we treated aged cells with the miR-92a mimic. Notably, there was a marked elevation in the expression of the OSKM members, particularly *SOX2*, *C-MYC*, and *KLF4*, in the miR-92a mimic treated aged hfNPCs (Fig. 5C). Given the observation from the hpEV treated cells, it is evident that, apart from *SOX2*, the expression of *C-MYC* and *KLF4* expressions were notably elevated. However, *OCT4* expression remained unchanged, suggesting that both the hpEV and the miR-92a mimic can influence a subset of OSKM to reactivate cells. The observed differences in expression patterns could potentially be attributed to the varying amounts of miR-92a mimic. To further confirm the involvement of the *TLR4* signaling pathway in the senescence of hfNPCs, we treated older hfNPCs with *TLR4* pathway inhibitors: CLI-095 or the downstream TRIF-TBK1 inhibitor BX-795 (Fig. 5D). We observed that treatment with CLI-095 remarkably reduced the transcription levels of $p16^{INK4a}$, $p19^{INK4d}$, $p21^{CIP1}$, and *p53* in older hfNPCs (Fig. 5E). Moreover, administering BX795 resulted in a significant increase in the expression of OSKM and *RBBP5* in older hfNPCs (Fig. 5F). These findings strongly suggest that *TLR4* pathway modulates cellular senescence by influencing the expression of OSKM

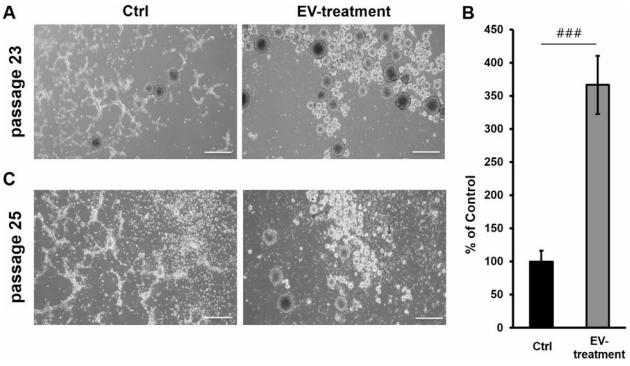

Fig. 6 Effect of hpEV treatment on neurosphere formation of old hfNPCs in non-adherent culture. (**A**) Representative images of neurospheres formed at Day 3 of suspension culture in passage 23 old hfNPCs untreated and 2 μg/ml hpEV-treated. Scale bar = 500 μm (**B**) Quantification of the number of neurospheres in panel A (**C**) Representative images of neurospheres formed at Day 5 of suspension culture in passage 25 old hfNPCs untreated and 2 μg/ml hpEV-treated. Scale bar = 500 μm. Data are presented as mean ± SD. ###: p values for comparison between Old control and Old EV-treatment groups, ### <0.001

in neural stem/progenitor cells and participating in an inflammatory signaling pathway [44].

Observing existence of *OCT4* and *C-MYC* mRNA in the hpEVs (Fig. S3), we further dissect the potential mechanisms underlying the hpEV mediated anti-senescence effects, especially the transfer of OSKM mRNAs. To facilitate EV-mediated gene transfer, a method was developed utilizing a cell-penetrating complex, specially employing a cell-penetrating peptide (CPP) fused with DNA binding peptide. GFP plasmids were successfully introduced into hpEVs using CPPs. To ascertain the effectiveness of our CPP-aided nucleotide transfer, we subsequently exposed older hfNPCs to the hpEVs infused with the GFP plasmid. This not only validated our method's robustness but also provided a foundation for deeper explorations into the dynamics of EV-mediated gene transfers in the realm of cellular aging. Compared to the control group without CPPs, the older hfNPCs treated with CPPs exhibited notably stronger green signals, with GFP proteins primarily localized in the cytoplasm. This observation indicates the successful transfer of plasmids into the cells (Fig. 5G). Next, we treated older hfNPCs with hpEVs loaded with a human *OCT4* plasmid for 96 h and found that the transferred *OCT4* plasmid significantly induced the expression of *SOX2*, *C-MYC*, *RBBP5*, and *OCT4* itself (Fig. 5H). In addition, human *SOX2* plasmids were transferred to the old hfNPCs after loaded into hpEVs. After 96 h incubation, all OSKM and *RBBP5* were significantly induced, especially the highest increase in *OCT4* expression (Fig. 5I), suggesting that either transferring or inducing OSKM (Fig. 5B) is able to reactivate PTFs and to rejuvenate aged hfNPCs. The results from both the miR-92a mimic and the plasmid transfers suggest a putative underlying mechanism of the hpEV mediated cellular rejuvenation. Stem cells, during their growth phase leading to senescence, exhibit elevated *TLR4* levels on their plasma membrane, which act as a catalyst for cellular aging. A primary contributor to this aging process is the *TLR4*-TBK1 pathway. This pathway substantially suppresses the expression of PTFs, OSKM, mainly by inhibiting *RBBP5*, intensifying the cellular aging process. However, a significant intervention occurs when these aged cells come into contact with youthful stem cells or their EVs. Upon internalization, these EVs release miRNAs targeting not only *TLR4* but also its downstream molecules, thereby weakening the *TLR4*-driven signals. This event leads to the release of the previously suppressed OSKM factors in the aged cells, reigniting the genes crucial for cell proliferation, anti-aging, and rejuvenation. Moreover, EVs, either from vibrant stem cells or other young tissues, also contain mRNAs for OSKM, promoting the direct expression of PTFs. This multifaceted interaction revitalizes aged cells, effectively halting their aging progression (Fig. 7). Taken together, hpEVs are able to inhibit cellular senescence and rejuvenate hfNPCs by suppressing the *TLR4* signal via miRNAs, followed by the induction of OSKM expression and the suppression of aging-related genes.

Discussion

Our study delves into the potential of hpMSCs as a solution for addressing neural aging, with a particular focus on their EVs. Through the multiple administrations of hpMSCs, we observed significant improvements in the survival and cognitive functions of aged mice. RNA sequencing analysis provided valuable insights into the influence of hpMSCs on aging-related neural pathways, notably highlighting the downregulation of age-related and oxidative stress indicating antioxidant genes in the hippocampus. Despite the challenges posed by hpMSCs in crossing the blood-brain barrier (BBB), their role in regenerating the aging brain via human hpEVs is pivotal. *Consistent with previous findings on BBB disruption during aging, we observed that hpEVs and tracer signals successfully penetrated into the brain parenchyma of aged mice but not young mice, further validating the feasibility of systemic EV delivery for neuroregenerative interventions in aging.* Recent research has highlighted the role of circulating EVs in young blood, particularly in regenerating aged skeletal muscle through the transfer of genetic materials, specifically mRNA. Notably, removing EVs from young blood compromised their beneficial effects [45]. Our study also indicates that both hpMSCs and hpEVs can suppress or delay normal cellular senescence in old neural progenitor cells (Fig. 2G-I and Fig. 3D). This suggests that the anti-aging effects mediated by hpMSCs are, at least in part, attributed to the released EVs, further underscoring their role in regenerative processes.

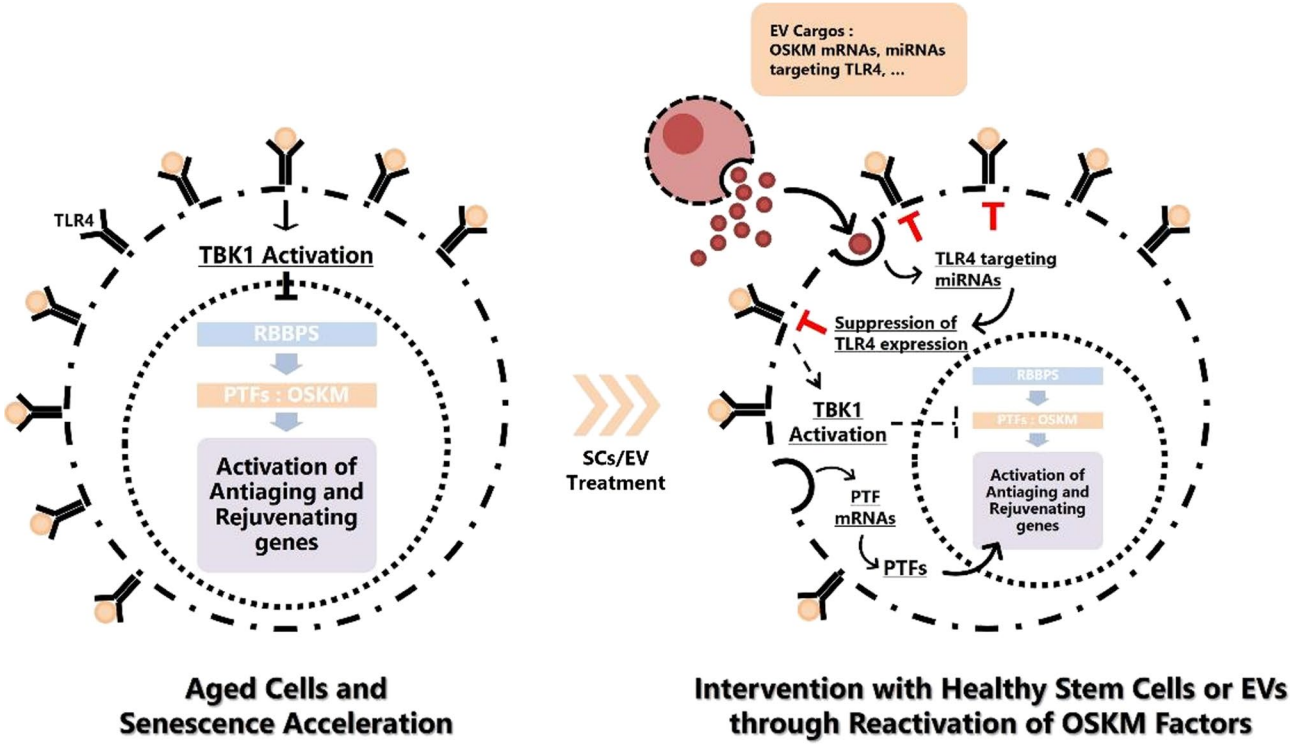

Fig. 7 Multi-faceted Role of EVs: Hypothetical Anti-Aging Mechanism. As stem cells proliferate and progress towards senescence, *TLR4* levels on the plasma membrane amplify, accelerating cellular aging. The *TLR4*-TBK1 pathway robustly inhibits the expression of pluripotent transcription factors, OSKM, primarily through the suppression of *RBBP5*, further exacerbating cellular senescence. However, when aged cells interact with healthy, young stem cells or their extracellular vesicles (EVs, represented as orange closed circles), the endocytosed EVs discharge miRNAs that target *TLR4* and its subsequent molecules, attenuating *TLR4* expression and its associated signaling pathways. As a result, the OSKM factors within the aged cells are liberated from the *TLR4*-associated inhibition. This reinvigorates old cells by reactivating target genes responsible for proliferation, anti-aging, and rejuvenation. EVs, whether derived from stem cells or other young, healthy cells/tissues, might not only carry diverse miRNAs modulating *TLR4* signaling but also house mRNAs coding for OSKM, elevating the expression of PTFs directly. Consequently, aged cells undergo rejuvenation, stalling the aging process. Green closed circle: *TLR4* ligand; Orange closed circle: EVs from young healthy stem cells; Black and Red T bars: inhibition of signal pathways; Dashed arrow: suppressed signals

Recent results support that miRNAs in stem cell-derived EVs play key roles in tissue recovery processes by modulating gene expression in various tissues [17–21]. Our analysis of small RNAs from hpEVs revealed the presence of numerous miRNAs targeting *TLR4* signaling implicated in aging and cellular senescence (Fig. 7). The hsa-miR-92a-3p, one of the highly enriched miRNAs in hpEVs, likely modulates the *TLR4*-mediated inflammasome pathway and activate pluripotent OSKM expression in aged cells and organs (Fig. 4 and Fig. 5C). This provides new insights into stem cell/stem cell-derived EV-mediated modulation of the *TLR4*-implicated aging process. While our data highlight TLR4 as a representative and tractable signaling node influenced by hpEV-derived miRNAs, it is important to note that the overall anti-senescence effects of hpEVs may involve additional inflammatory or aging-associated pathways (e.g., other TLRs, NF-κB, NLRP3). Further studies using broad signaling inhibition and network-level analyses will be needed to delineate the full spectrum of downstream pathways modulated by hpEVs. Their role in suppressing *TLR4* signaling while upregulating OSKM transcription factors was further assessed. In aged stem cells and non-stem cells, the activation of *TLR4* dimers inhibits OSKM activation by suppressing *RBBP5* expression. In contrast, young stem cells release EVs containing miRNAs that target *TLR4*, effectively suppressing its expression. When these EVs fuse with their target cells, the transferred miRNAs relieve the *TLR4*-induced repression of OSKM. As a result, OSKM factors becomes reactivated, which is associated with the observed partial recovery of these senescent cells (Fig. 7), although this correlation dose not prove causation. These results may be attributed to the inherent characteristics of hfNPCs. It's worth noting that *SOX2*, a marker commonly associated with neural stem cells (NSCs) and neural progenitor cells (NPCs), is typically highly expressed in NPCs, and able to induce the expression of endogenous pluripotent transcription factors (PTFs), subsequently regulating their target genes and maintaining the induced pluripotent stem cell (iPSC) state, all without the need for additional exogenous factors [43]. Given these insights, the induction of *SOX2* by hpEVs within a four-day timeframe may indicate that the senescent hfNPCs under treatment are in the early stages

of reactivation. The potent effect of *SOX2* is evident from our EV-loading experiment, which showed reactivation of all OSKM factors accompanied by signs of senescent cell rejuvenation (Fig. 5I). It's plausible that the hpEV mediated induction or transfer of SOX2 may require a longer duration to progress to a later stage of the PSC process, facilitated by *SOX2*-mediated activation of other factors. This transient reactivation strategy is consistent with previous reports demonstrating that short-term (2–4 days) induction of OSKM factors can restore youthful gene expression and tissue function without tumorigenic transformation (Ocampo et al., 2016; EMBO Mol Med, 2017). Our hpEV-based approach likewise promotes partial reprogramming over a brief period, thereby minimizing oncogenic risk. Additionally, it's important to consider that EVs may carry OSKM mRNAs and proteins themselves, as evidenced by the detection of OCT4 and C-MYC genes (Fig. S3). These transferred OSKM mRNAs and proteins can directly and transiently induce the expression of other PTFs and reactivate aged cells independently of TLR4 signals, which is supported by the observed OCT overexpression in this study (Fig. 5H). While these experiments demonstrate the feasibility of using hpEVs as gene delivery vehicles, we acknowledge that the CPP-assisted loading of exogenous plasmids does not reflect the native physiological mechanism of hpEV cargo transfer. Rather, this approach was employed as a functional test to explore the application potential of engineered hpEVs for exogenous gene modulation. This distinction is important to separate mechanistic findings based on native hpEV action from translational strategies that harness their delivery capacity. As a result, stem cells or stem cell-derived EVs have the potential to delay or inhibit the aging processes in endogenous stem cells and somatic cells, or even regenerate them.

Interestingly, our study aligns with recent research demonstrating that the aging-related proteins, which increase in both Old mice and humans, can be effectively suppressed by infusing human umbilical cord plasma [3]. This treatment not only improved hippocampal and cognitive functions in aged mice but also increased the expression of tissue inhibitor of metalloproteinases 2 (*TIMP2*), a molecule linked to spatial memory and long-term potentiation. The authors analyzed the youth related factors, including *TIMP2*, in human cord blood plasma and plasma from different aged mice and then revealed the age dependent separation of proteins and the putative regenerating factors in human cord blood plasma. Intriguingly, our findings mirror the changes observed between the youth-associated proteins from human cord blood plasma and their expression in the hippocampus treated with hpMSCs: there was an hpMSC associated induction of proteins that had decreased in aged individuals but upregulated in the cord blood plasma (Table S5). These parallels strongly suggest the hpMSC treatment modulate an age implicated environment in organisms toward a more youthful condition, which is the common mechanism between human cord blood and hpMSC-mediated anti-aging effects.

In this study, we focused on female C57BL/6 mice and did not assess the therapeutic effects of hpMSCs in males. Our findings indicate that the therapeutic potential of hpMSCs may be influenced by sex-related differences, such as estrous cycle variations and hormonal levels. Female C57BL/6 mice are known to exhibit more pronounced cognitive deficits due to natural aging compared to males. Additionally, studies have shown that despite estrous cycle variations, female C57BL/6 mice display a more consistent pattern of aging-related changes than males, making them a suitable model for our study. Although we did not perform behavioral tests on male C57BL/6 mice, we observed neuroregenerative effects of hpEVs in these males. This suggests that hpMSCs or hpEVs could potentially offer similar regenerative benefits in aging male C57BL/6 mice. We are currently conducting a comprehensive in vivo study that includes males to further explore this hypothesis. These findings highlight the broad applicability of hpMSCs and hpEVs for neuroregeneration across both sexes, reinforcing their potential as therapeutic agents for age-related conditions. For clinical translation, key considerations will include the scalability and standardization of hpEV production, quality control across donor batches, and the need for comprehensive safety assessment—including biodistribution, immunogenicity, and long-term oncogenic risk evaluation—prior to human application.

In conclusion, our study showed that hpMSCs and hpEVs can reactivate endogenous stem cells and improve cellular function and individual's activities via modulating various age- and anti-stress-related genes. The anti-aging effect of hpMSCs is, at least partially, mediated by EVs that deliver miRNAs and/or mRNAs to compromise *TLR4* signals and to modulate both the aging/cellular senescence process and inflammation status. Our research has pioneered a groundbreaking strategy for regenerating neural aging through two distinct approaches: (1) hpEVs and (2) hpEV-mediated OSKM stimulation, which offers the potential to amplify the therapeutic effect. While OSKM factor upregulation coincides with improved function in our aging model, our data do not establish a direct causal relationship. Definitive proof would require targeted loss-of-function experiments (e.g., OSKM knockdown or pathway blockade in vivo) to determine whether abrogating OSKM activity diminishes the observed benefits. Our findings underscore the transformative potential of EV-based therapies in the realm of anti-aging interventions and support clearly that the role of EVs, and the miRNAs

they harbor, is central to our quest for interventions that can extend health span and enhance the quality of life in aging individuals.

Conclusion

In conclusion, our study showed that hpMSCs and hpEVs can reactivate endogenous stem cells and improve cellular function and individual's activities via modulating various age- and anti-stress-related genes. The anti-aging effect of hpMSCs is, at least partially, mediated by EVs that deliver miRNAs and/or mRNAs to compromise TLR4 signals and to modulate both the aging/cellular senescence process and inflammation status. Our research has pioneered a groundbreaking strategy for regenerating neural aging through two distinct approaches: (1) hpEVs and (2) hpEV-mediated OSKM stimulation, which offers the potential to amplify the therapeutic effect. Our findings underscore the transformative potential of EV-based therapies in the realm of anti-aging interventions and support clearly that the role of EVs, and the miRNAs they harbor, is central to our quest for interventions that can extend health span and enhance the quality of life in aging individuals.

Abbreviations

AD	Alzheimers disease
APP	Amyloid precursor protein
BBB	Blood-Brain barrier
CAT	Catalase
CM	Conditioned media
CPP	Cellpenetrating peptide
ddG	Delta delta G
EVs	Extracellular vesicles
GFAP	Glial fibrillary acidic protein
hfNPCs	Human fetal neural progenitor cells
HMGA2a	High mobility group ATHook 2a
hpEVs	Human placenta-derived extracellular vesicles
hpMSCs	Human placenta-derived mesenchymal stem cells
iPSCs	Induced pluripotent stem cells
MSCs	Mesenchymal stem cells
MWM	Morris water maze
NLRP3	NOD-like receptor family pyrin domain containing 3
NRF2	Nuclear factor erythroid 2related factor 2
NTA	Nanoparticle tracking analysis
OSKM	OCT4 SOX2 KLF4 and CMYC
PCNA	Proliferating cell nuclear antigen
PD	Parkinsons disease
PTFs	Pluripotent transcripton factors
RBBP5	RB binding protein 5
SOD1	Superoxide dismutase 1
SOD2	Superoxide dismutase 2
TEM	Transmission eletron microscopy
TIMP2	Tissue inhibitor of metalloproteinases 2
TLR4	Toll-like receptor 4
TRIL	TLR4 interactor with leucinerich repeats
TUJ-1	Class III beta-tubulin

Supplementary Information

The online version contains supplementary material available at https://doi.org/10.1186/s12964-025-02469-5.

Supplementary Material 1: Supplemental Figure 1. Senescence Assessment of Human Fetal Neural Progenitor Cells. (A) Change in the proliferation rates of hfNPCs was monitored from passage 15 (p15) to passage 30 (p30). The proliferation of hfNPCs began to decrease around passages 22-23 and came to a halt between p27-28, accompanied by cell death. (B) Expression levels of proliferation marker, ***PCNA*** diminished over successive passages and conversely, senescence associated $p16^{INK4a}$ expression increased over successive passages. (C) The morphological features of hfNPCs underwent noticeable changes as the passage number increased. (D) The spontaneous differentiation capacity in mid-aged and old-aged hfNPCs was evaluated. The expression of TUJ-1 at p25 decreased compared to p17. Scale bar: 100. Supplemental Figure 2. Image of plam-tdTomato infected hpMSCs and cell injected mouse. (A) Representative confocal image of hpMSCs infected with plam-tdTomato. The infection of hpMSCs with plam-tdTomato is demonstrated by the detected tdTomato (Red). The scale bar represents 20 μm. (B) Representative confocal image of a mouse brain treated with plam-tdTomato-hpMSCs. This image shows the migration of EVs released from intravenously injected hpMSCs into the brain. This is evidenced by the detected tdTomato (Red) and human CD63 (Green) in the brain. The scale bar represents 100 μm). Supplemental Figure 3. Existence of pluripotent transcription factors, ***OCT4*** and ***C-MYC*** in the extracellular vesicles from various sources.***OCT4*** and***C-MYC*** mRNAs were detected in the total RNAs inside extracellular vesicles from various human sources. Abbreviations: hfNPC-EVs — human fetal neural progenitor cells derived EVs; hpMSCs-EVs —EVs isolated from culture media of human placenta derived mesenchymal stem cells; hPEVs —human placenta tissue derived EVs; hCEVs —human cord tissue derived EVs. Table S1. Gene Ontology (GO) Analysis Comparing 'Old' and 'Young' Groups. Table S2. Inhibition or Activation of Neuronal Function-Related Genes in Old Mice. Table S3. Gene Ontology (GO) Analysis of aged Old control vs. hpMSC-Treated Old mice. Table S4. RNA-Seq Analysis: Differentially Expressed Genes in the Hippocampi of hpMSC-Treated Old Mice. Table S5. Comparative Analysis of RNA-Seq Results from hpMSC-Treated (hpMSC-T) and protein analysis from human umbilical cord blood plasma-Treated (hUCBP-T) Old mice. Table S6. List of Primers Used in the Study.

Acknowledgements

We thank Ph.D. Do Won Hwang of Seoul National University for producing and providing the palm-tdTomato lentivirus.

Authors' contributions

Chul Kim carried out the Conceptualization, Methodology, Investigation, Project administration, and Writing-Original draft. Soo-Hyeon Nam and Chul-Woo Lim carried out the Experiments, and Writing-Review and Editing. Jae Hyun Park carried out the Experiments, Statistical Analysis, and Writing-Review and Editing. Yun-Hwa Jeong carried out the Statistical Analysis. Jin Young Lee carried out the Methodology, Experiments, and Writing-Review and Editing. Youngsook Song and Seungmin Lee carried out the Investigation, Experiments, and Writing-Original draft. Moonbeom Choi carried out the Experiments. Ji Hyung Chung carried out Methodology. Jisook Moon carried out the Conceptualization, Methodology, Investigation, Project administration, Writing-Original draft, and Writing-Review and Editing.

Funding

This work was supported by the National Research Foundation of Korea (NRF) grant funded by the Korea government (MSIT) (RS-2024-00462182).

Data availability

RNA sequencing data were deposited into the Gene Expression Omnibus database under accession number GSE305309 and GSE305310.

Declarations

Ethics approval and consent to participate

All animal studies were performed in compliance with Institutional Animal Care and Use Committee (IACUC) at CHA University. The reference number of the approvals of the animal study is IACUC150007.

Consent for publication

Not applicable.

Competing interests
The authors declare no competing interests.

Received: 7 April 2025 / Accepted: 30 September 2025
Published online: 29 October 2025

References

1. López-Otín C, Blasco MA, Partridge L, Serrano M, Kroemer G. The hallmarks of aging. Cell. 2013;153:1194.
2. López-Otín C, Galluzzi L, Freije JMP, Madeo F, Kroemer G. Metabolic Control Longev Cell. 2016;166:802–21.
3. Castellano JM, Mosher KI, Abbey RJ, Mcbride AA, James ML, Berdnik D, Shen JC, Zou B, Xie XS, Tingle M, Hinkson IV, Angst MS, Wyss-Coray T, Mosher KI, Abbey RJ, McBride AA, James ML, Berdnik D, Shen JC, ZouNature B. 2017•nature Com. 2017;544:488–92.
4. Childs BG, Durik M, Baker DJ, van Deursen JM. Cellular senescence in aging and age-related disease: from mechanisms to therapy. Nat Med. 2015;21:1424–35. https://pubmed.ncbi.nlm.nih.gov/26646499/.
5. Pilzecker B, Buoninfante OA, Pritchard C, Blomberg OS, Van Den Huijbers IJ, Jacobs H, Pilzecker OA, Buoninfante C, Pritchard OS, Blomberg IJ, Huijbers. 2016•academic Oup Com. 2016;44:4734–44. PCM van den BerkNucleic acids research.
6. Duncan T, Valenzuela M. Alzheimer's disease, dementia, and stem cell therapy. 2017•Stem Cell Res Ther. 8(1):111. https://pubmed.ncbi.nlm.nih.gov/28494803/.
7. Fiedler A, Grecksch G, Reinhold A, Schraven B, Becker A. Hippocampus-dependent learning in SKAP-HOM deficient mice. Behav Brain Res. 2014;270:125–30.
8. Gugliandolo A, Bramanti P, Mazzon E. Mesenchymal stem cell therapy in parkinson's disease animal models. Curr Res Transl Med. 2017;65:51–60.
9. Medhekar SK, Shende VS, Chincholkar AB. Recent stem cell advances: cord blood and induced pluripotent stem cell for cardiac regeneration- a review. Int J Stem Cells. 2016;9:21–30.
10. Kim KS, Kim HS, Park JM, Kim HW, Park Mkyung, Lee HS, Lim DS, Lee TH, Chopp M, Moon J. Long-term Immunomodulatory effect of amniotic stem cells in an alzheimer's disease model. Neurobiol Aging. 2013;34:2408–20.
11. Kong T, Park J-M, Jang JH, Kim C-Y, Bae S-H, Choi Y, Jeong Y-H, Kim C, Chang SW, Kim J, Moon J.Immunomodulatory effect of CD200-positive human placenta-derived stem cells in the early phase of stroke.2018•Exp Mol Med. 50(1):e425. https://doi.org/10.1038/emm.2017.233, https://pubmed.ncbi.nlm.nih.gov/29328072/.
12. Kim C, Park J-M, Kong T, Lee S, Seo K-W, Choi Y, Song YS, Moon J. Double-Injected human stem cells enhance rehabilitation in TBI mice via modulation of survival and inflammation. Mol Neurobiol. 2018;55:4870–84. https://pubmed.ncbi.nlm.nih.gov/28736792/.
13. Pawitan JA. Prospect of stem cell conditioned medium in regenerative medicine. Biomed Res Int. 2014;2014:965849.
14. Lee M, Im W, Kim M. Exosomes as a potential messenger unit during heterochronic parabiosis for amelioration of huntington's disease. Neurobiol Dis. 2021;155:105374. https://pubmed.ncbi.nlm.nih.gov/33940179/.
15. Stoorvogel W, Kleijmeer MJ, Geuze HJ, Raposo G. The biogenesis and functions of exosomes. Traffic. 2002;3:321–30. https://pubmed.ncbi.nlm.nih.gov/11967126/.
16. Robbins PD. Extracellular vesicles and aging. Stem Cell Investig. 2017;4:98–98.
17. Zhang Y, Kim MS, Jia B, Yan J, Zuniga-Hertz JP, Han C, Cai D, Kim MS, Jia B, Yan J, Zuniga-Hertz JP, Han C, CaiNature D. 2017•nature Com. 2018;548:52–7.
18. Gai C, Carpanetto A, Deregibus M, Camussi G. Extracellular vesicle-mediated modulation of angiogenesis. Histol Histopathol. 2016;31:379–91.
19. Collino F, Bruno S, Incarnato D, Dettori D, Neri F, Provero P, Pomatto M, Oliviero S, Tetta C, Quesenberry PJ, Camussi G. AKI recovery induced by mesenchymal stromal cell- derived extracellular vesicles carrying Micrornas. J Am Soc Nephrol. 2015;26:2349–60.
20. Tan CY, Lai RC, Wong W, Dan YY, Lim S-K, Ho HK. Mesenchymal stem cell-derived exosomes promote hepatic regeneration in drug-induced liver injury models. Stem Cell Res Ther. 2014;5:76. https://pubmed.ncbi.nlm.nih.gov/24915963/.
21. Lai RC, Arslan F, Lee MM, Sze NSK, Choo A, Chen TS, Salto-Tellez M, Timmers L, Lee CN, El Oakley RM, Pasterkamp G, de Kleijn DPV, Lim SK. Exosome secreted by MSC reduces myocardial ischemia/reperfusion injury. Stem Cell Res. 2010;4:214–22.
22. Strong R, Miller RA, Astle CM, Baur JA, De Cabo R, Fernandez E, Guo W, Javors M, Kirkland JL, Nelson JF, Sinclair DA, Teter B, Williams D, Zaveri N, Nadon NL, Harrison DE. Evaluation of resveratrol, green tea extract, curcumin, oxaloacetic acid, and medium-chain triglyceride oil on life span of genetically heterogeneous mice. Journals Gerontol - Ser Biol Sci Med Sci. 2013;68:6–16.
23. Austad SN, Fischer KE. Sex differences in lifespan. Cell Metab. 2016;23:1022–33 https://pubmed.ncbi.nlm.nih.gov/27304504/.
24. Bae S-H, Lee H-S, Kang M-S, Strupp BJ, Chopp M, Moon J. The levels of pro-inflammatory factors are significantly decreased in cerebral palsy patients following an allogeneic umbilical cord blood cell transplant. Int J Stem Cells. 2012;5:31–8. https://pubmed.ncbi.nlm.nih.gov/24298353/.
25. Lee EJ, Choi Y, Lee HJ, Hwang DW, Lee DS. Human neural stem cell-derived extracellular vesicles protect against Parkinson's disease pathologies. J Nanobiotechnol. 2022;20:198. https://pubmed.ncbi.nlm.nih.gov/35468855/.
26. Moon J, Schwarz SC, Lee H-S, Kang JM, Lee Y-E, Kim B, Sung M-Y, Höglinger G, Wegner F, Kim JS, Chung H-M, Chang SW, Cha KY, Kim K-S, Schwarz J. Preclinical analysis of fetal human mesencephalic neural progenitor cell lines: characterization and safety in vitro and in vivo. Stem Cells Transl Med. 2017;6:576–88. https://pubmed.ncbi.nlm.nih.gov/28191758/.
27. Trapnell C, Pachter L, Salzberg SL. TopHat: discovering splice junctions with RNA-Seq. Bioinformatics. 2009;25:1105–11. https://pubmed.ncbi.nlm.nih.gov/19289445/.
28. Dennis G, Sherman BT, Hosack DA, Yang J, Gao W, Lane HC, Lempicki RA. DAVID: database for Annotation, Visualization, and integrated discovery. Genome Biol. 2003;4(5):P3.
29. Liao Y, Smyth GK, Shi W. The Subread aligner: fast, accurate and scalable read mapping by seed-and-vote. Nucleic Acids Res. 2013;41:e108. https://pubmed.ncbi.nlm.nih.gov/23558742/.
30. Wang X. miRDB: a microRNA target prediction and functional annotation database with a wiki interface. RNA. 2008;14:1012–17.
31. Narita M, Narita M, Krizhanovsky V, Nuñez S, Chicas A, Hearn SA, Myers MP, Lowe SW. A novel role for High-Mobility group A proteins in cellular senescence and heterochromatin formation. Cell. 2006;126:503–14.
32. Fernandes Bondan E, Cardoso CV, De Fátima M, Martins M, Otton R. Memory impairments and increased GFAP expression in hippocampal astrocytes following hypercaloric diet in rats. SciELO BrasilEF Bondan CV Cardoso MFM Martins R OttonArquivos De Neuropsiquiatr. 2019;77:601–8. SciELO Brasil 2019.
33. Kandlur A, Satyamoorthy K, Gangadharan G. Oxidative stress in cognitive and epigenetic aging: a retrospective glance. Front Mol Neurosci. 2020;13:41. https://pubmed.ncbi.nlm.nih.gov/32256315/.
34. Phillips TJ, Kamens HM, Wheeler JM. Behavioral genetic contributions to the study of addiction-related amphetamine effects. Neurosci Biobehav Rev. 2008;32:707–59. https://pubmed.ncbi.nlm.nih.gov/18207241/.
35. Nagler RM. Salivary glands and the aging process: mechanistic aspects, health-status and medicinal-efficacy monitoring. Biogerontology. 2004;5:223–33.
36. Lai CP, Kim EY, Badr CE, Weissleder R, Mempel TR, Tannous BA, Breakefield XO. Visualization and tracking of tumour extracellular vesicle delivery and RNA translation using multiplexed reporters. Nat Commun. 2015;6:7029. https://pubmed.ncbi.nlm.nih.gov/25967391/.
37. Caravia XM, López-Otín C. Regulatory roles of MiRNAs in aging. Adv Exp Med Biol. 2015;887:213–30.
38. Kinser HE, Pincus Z. MicroRNAs as modulators of longevity and the aging process. Hum Genet. 2020;139:291–308. https://pubmed.ncbi.nlm.nih.gov/31297598/.
39. Yang J, Wise L, Fukuchi K-I. TLR4 cross-talk with NLRP3 inflammasome and complement signaling pathways in Alzheimer's disease. Front Immunol. 2020;11:724. https://pubmed.ncbi.nlm.nih.gov/32391019/.
40. Momtazmanesh S, Perry G, Rezaei N. Toll-like receptors in Alzh eimer's disease. J Neuroimmunol. 2020;348:577362. https://pubmed.ncbi.nlm.nih.gov/32858428/.
41. Alvarado AG, Thiagarajan PS, Mulkearns-Hubert EE, Silver DJ, Hale JS, Alban TJ, Turaga SM, Jarrar A, Reizes O, Longworth MS, Vogelbaum MA, Lathia JD. Glioblastoma cancer stem cells evade innate immune suppression of Self-Renewal through reduced TLR4 expression. Cell Stem Cell. 2017;20:450–e4614.
42. Qin ZY, Gu X, Chen YL, Liu JB, Hou CX, Lin SY, Hao NN, Liang Y, Chen W, Meng HY. Toll-like receptor 4 activates the NLRP3 inflammasome pathway and periodontal inflammaging by inhibiting Bmi-1 expression. Int J Mol Med. 2021;47:137–50.

43. Zhang S, Cui W. Sox2, a key factor in the regulation of pluripotency and neural differentiation. World J Stem Cells. 2014;6:305–11. https://pubmed.ncbi.nlm.nih.gov/25126380/.
44. Kawasaki T, Kawai T. Toll-like receptor signaling pathways. Front Immunol. 2014;5:461. https://pubmed.ncbi.nlm.nih.gov/25309543/.
45. Sahu A, Clemens ZJ, Shinde SN, Sivakumar S, Pius A, Bhatia A, Picciolini S, Carlomagno C, Gualerzi A, Bedoni M, Van Houten B, Lovalekar M, Fitz NF, Lefterov I, Barchowsky A, Koldamova R, Ambrosio F. Regulation of aged skeletal muscle regeneration by circulating extracellular vesicles. Nat Aging. 2021;1:1148–61. https://pubmed.ncbi.nlm.nih.gov/35665306/.

Publisher's note